

Complex Memory Formation in Frictional Granular Media

D. Candela*

Physics Department, University of Massachusetts, Amherst MA 01003

(Dated: April 26, 2023)

Using numerical simulations it is shown that a jammed, random pack of soft frictional grains can store an arbitrary waveform that is applied as a small time-dependent shear while the system is slowly compressed. When the system is decompressed at a later time, an approximation of the input waveform is recalled in time-reversed order as shear stresses on the system boundaries. This effect depends on friction between the grains, and is independent of some aspects of the friction model. This type of memory could potentially be observable in other types of random media that form internal contacts when compressed.

There are many forms of memory in condensed matter, i.e. ways in which inputs applied over one time period can appear as measurable outputs at later times [1]. Here it is shown using simulations that the elastic properties of a granular medium – a random pack of μm or larger size particles with contact interactions – can be used to encode arbitrary waveform data, store it for long times, and (imperfectly) recall the data when desired. Similar waveform memory might be observable in other systems that share key properties with granular media such as fiber nests [2], fiber bundles and yarns [3, 4], textiles [5], and crumpled sheets [6–8]. This type of effect is broadly interesting as it shows that a detailed record of past events can, surprisingly, sometimes be stored and read out from “ordinary” random media not designed for the purpose.

A variety of memory effects have been found previously in amorphous many-particle systems. For example, multiple shear values can be stored via cyclic training in both suspensions [9] and model glasses [10–12]. Granular media can also be trained by cyclic shearing [13–16] and store information on shear history in the fabric of force chains [17]. Nonlinear acoustic modes of granular media give rise to time-domain echoes [18].

The memory effect reported here differs from most of these earlier results as the input data are stored and later recalled with a single cycle of the control variable. The memories are complex in the sense that they approximately store an entire time-dependent waveform that could eventually represent, for example, a spoken word. In simulations the memories are stored indefinitely, but in physical systems creep [19] might limit storage times.

Many of the unusual mechanical and acoustic properties of granular media can be traced to the network of contacts between grains [20–22]. Additional contacts are formed as the sample is compressed beyond the jamming point, and a large system always includes contacts close to forming or separating [23, 24]. When there is contact friction the forces depend upon the path by which the granular system reaches a given state, creating possibilities for memory effects [25–27].

Simulated system.—Parameters were chosen that could be recreated in physical experiments. A non-spherical grain shape was used, modeled for simplicity [28, 29] by

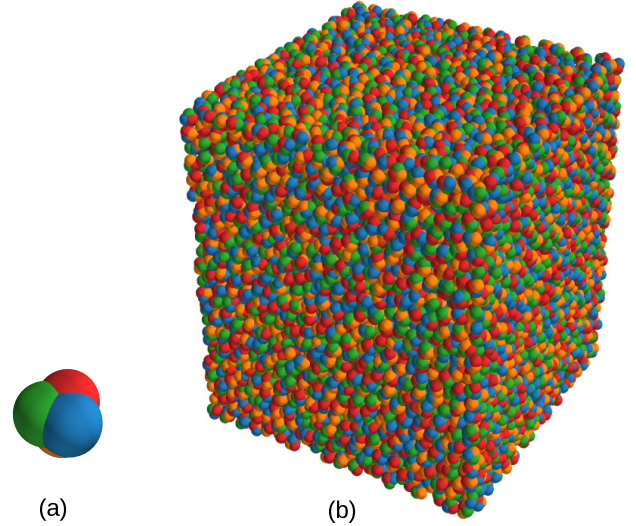


FIG. 1. (a) A single grain, which has the exterior shape of four partially overlapping spheres. The sphere centers are at the vertices of a tetrahedron with edge length 40% of the sphere diameter. (b) Random pack of 10 240 such grains (confining walls not shown).

four tetrahedrally-arranged partially overlapping spheres of radius $R = 0.5$ mm (Fig. 1(a)) with the properties of silicone rubber (density $\rho = 1.2 \times 10^3$ kg/m³, Young modulus $E = 1.0 \times 10^7$ Pa, Poisson ratio $\nu = 0.49$, friction coefficient $\mu \approx 1.0$). A soft elastomer like this can withstand strains of several percent, as used in the simulations. A characteristic time from these parameters is $t_c = R(\rho/E)^{1/2}$, which is about one-tenth the period of the highest-frequency vibrational mode of a moderately compressed pack of these grains.

As detailed below the contact forces are modeled by a Hertzian repulsive normal force along with three successively more realistic friction force models denoted H, M1, M2. Apart from M2 these models have commonly been used to simulate granular media.

Conventional discrete element method (DEM) methods [30–34] were used to integrate the equations of motion for n_g grains with these forces, confined by friction-

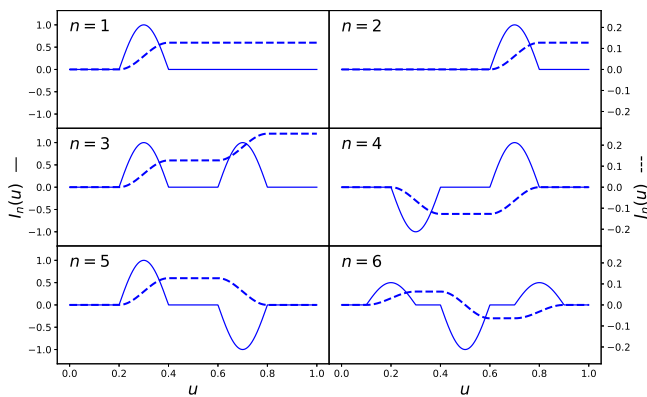


FIG. 2. Six input waveforms $I_n(u)$ used for memory trials (additionally $I_0(u) = 0$ was used). Each waveform is composed of up to three half-cycle cosine curves. Shear strain proportional to $I_n(u)$ was applied to the sample (solid curves), but the shear stress recalled later was found to be proportional to the integral of the strain $J_n(u) = \int_0^u I_n(v)dv$ (dashed curves).

less walls. The data shown here are for $n_g = 10240$, but the memory effect is visible at reduced fidelity for n_g as small as 325. An integration time step $\Delta t \leq (0.4)t_c$ gave numerical stability, requiring of order 10^6 steps.

Sample preparation.—An initial simulation was used to prepare the packed granular sample. The grains were placed in a rectangular box on a low-density lattice with random velocities, and allowed to evolve to randomize positions and orientations [36]. Then with the $+z$ wall free to move an external pressure $p_z = (2 \times 10^{-3})E$ was used compress the grains into an approximately cubical pack, Fig. 1(b). After the system to come nearly to rest the $\pm z$ walls were fixed in place while the $\pm x, \pm y$ walls were used to compress and decompress the sample two times mimicking the compression cycles used later in the experiment simulations. The grain-grain friction coefficient μ was set to zero during this entire sample preparation procedure [36–38].

Memory experiments.—A single sample prepared as above was used as the starting point for multiple memory-experiment simulations using different shear input waveforms. For these simulations μ was set to the chosen value (1.0 except as noted). To exhibit the memory effect, the grain pack was slowly and linearly compressed, while simultaneously applying an arbitrary input waveform as a small shear strain. The compression was applied by moving the four walls $\pm x, \pm y$ inward simultaneously and linearly in time over a period $t_0 = (1.8 \times 10^4)t_c$, to change the sample volume by $\Delta V/V = -\delta_0 = -0.05$. The average coordination number (contacts on a grain) Z increased from 9.0 to 10.4 as the sample was compressed, remaining between the frictional ($Z = 4$) and frictionless ($Z = 12$) isostatic values [39–41]. The the inertial number $I = \dot{\epsilon}\sqrt{m/Dp}$ (with

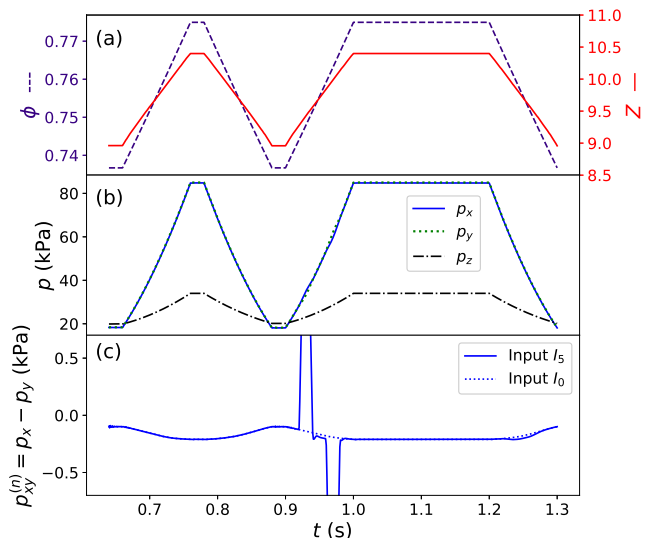


FIG. 3. Quantities versus time t for a memory experiment using input signal I_5 . The the sample preparation period with zero friction $t < 0.64$ s is not shown; friction is turned on for the entire period shown here. After a preparatory compression cycle (0.68 s - 0.88 s), the sample is compressed while the input signal I_5 is applied as an x - y shear strain (0.9 s - 1.0 s), held compressed for a storage period (1.0 s - 1.2 s), and finally decompressed to read out the memory response (1.2 s - 1.3 s). (a) Sample filling factor $\phi(t)$ and average coordination number $Z(t)$. Note tetrahedral particles typically pack more densely than spheres [35]. (b) Pressures on the x , y , and z walls. The responses of p_x, p_y to the input signal are barely visible during the encoding period 0.9 s - 1.0 s. (c) Difference between p_x and p_y on an expanded vertical scale, shown both when input I_5 is applied and when the zero-shear input I_0 is applied. Now the response to I_5 during the encoding period is readily visible, while differences between the responses to I_5 and I_0 are barely visible during the readout period 1.2 s - 1.3 s.

$\dot{\epsilon}$ the strain rate, m, D the grain mass and diameter, and p the pressure) was always less than 4×10^{-5} , giving a nearly quasistatic compression [24, 42].

The compression was parameterized by a variable $u(t)$ that went from zero to one as the sample was compressed, then back to zero when the sample was decompressed. The sample was compressed and decompressed once without applied shear. Then, during the course of a final compression, an input was applied by small additional movements of the $\pm x$ walls inward while moving the $\pm y$ walls outward (or vice versa), so as to create a pure shear of the sample $\gamma(u) = \gamma_0 I_n(u)$. Here $\gamma_0 = 10^{-3}$ set the scale of the shear strain and $I_n(u), n = 0 \dots 6$ were seven different input waveforms with $-1 \leq I_n(u) \leq 1$ (Fig. 2), used for seven separate experiment simulations. The $I_n(u)$ were chosen as simple waveforms to minimally test the independent recall of multiple inputs in a single experiment.

It was found that the recalled shear-stress signal when

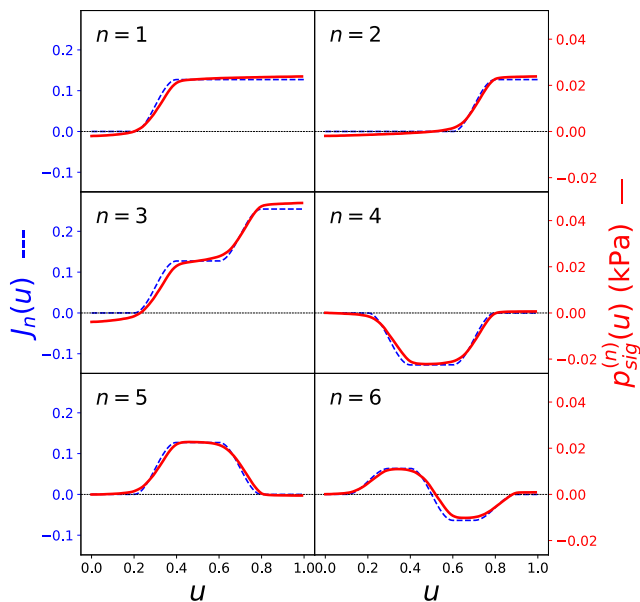


FIG. 4. Recalled signal $p_{sig}^{(n)}(u) = -(p_{xy}^{(n)} - p_{xy}^{(0)})$ when the sample is decompressed, for the six input signals $n = 1 \dots 6$ shown in Fig. 2 (solid lines). For comparison the dashed lines show the corresponding integrated shear inputs $J_n(u)$ applied earlier when the sample was compressed. A single gain factor $\mathcal{G} = 1.77 \times 10^5$ Pa was computed to minimize the least-squares difference between $\mathcal{G}\gamma_0 J_n(u)$ and $p_{sig}^{(n)}(u)$ summed over all six signals, and used to scale all plots equally.

the sample was decompressed was proportional not directly to the applied shear $I_n(u)$ but rather to its integral $J_n(u) = \int_0^u I_n(v)dv$. This emerges as well from a rough explanation for the memory effect presented below.

Simulation results.—Figures 3(b,c) show the pressures p_x, p_y, p_z measured on the sample walls during a typical simulation run, along with the shear stress $p_{xy} = p_x - p_y$ which has the symmetry of the applied input signals. While the response of $p_{xy}^{(n)}$ to the input signal $I_n(u)$ during compression is clearly visible, the recalled response when the sample is later decompressed is barely visible Fig. 3(c) due to the background signal observed even when no input signal is applied. This background reflects the x - y asymmetry of a specific random pack.

In Fig. 4 the zero-input background (measured in a separate simulation run) is subtracted to give the processed response signal $p_{sig}^{(n)} = -(p_{xy}^{(n)} - p_{xy}^{(0)})$. It can be seen that the response $p_{sig}^{(n)}(u)$ is nearly proportional to the input signal $J_n(u)$, demonstrating the postulated granular memory effect. A single parameter \mathcal{G} was adjusted to minimize the integrated least-squares difference between $\mathcal{G}\gamma_0 J_n(u)$ and $p_{sig}^{(n)}(u)$ summed over the entire suite shown in Fig. 4 [43].

Discrepancies between the recalled and input signals are also visible in Fig. 4. These suggest limits on the complexity of the memory that can be stored, possibly

related to the size of the granular system and the amplitude and/or frequency composition of the input signals. This will be the subject of future investigations.

During the storage period between encoding and recalling the signals the maximum grain velocity decayed exponentially towards the numerical noise floor, implying the signals could be stored indefinitely.

Dependence on the friction coefficient.— Additional simulations to be reported elsewhere were carried out with frictional sample preparation and/or spherical grains. It was found that both frictionless sample preparation and non-spherical grains as used for the results reported here tended to make the memory effect more visible, by reducing the frequency of large grain movements during compressions [44]. Similarly it was found in Ref. [45] that large grain movements destroy memory when a granular medium is sheared. However the parameter that appears most directly to control the ability to store memories is the friction coefficient μ , Fig. 5(a). This suggests that friction at contacts is the ultimate physical origin of this phenomenon.

Heuristic explanation of memory effect.—A rough explanation is as follows: At the point u during the compression at which a particular contact is formed, the grains coming into contact are displaced relative to one another by an amount proportional to the shear strain $\gamma_0 I_n(u)$ applied to the sample, and when this input strain is later removed there will be a corresponding transverse stress in the contact due to friction. At the end of the compression, the externally measurable wall stress $p_{xy}^{(n)}(u=1)$ should have contributions proportional to all such contact stresses, i.e. to $\gamma_0 \int_0^1 I_n(u)du = \gamma_0 J_n(1)$. During the decompression each contact stress is relieved at approximately the same point u at which the contact was formed, giving a contribution to $p_{xy}^{(n)}(u) \propto -\gamma_0 J_n(u)$.

For a quantitative theory, it would be necessary to connect the macroscopic applied strain $\gamma_0 I_n(u)$ to the distribution of transverse grain movements at contacts, and similarly to connect grain-scale friction forces to the macroscopic wall stress $p_{xy}^{(n)}(u)$. This is nontrivial due to non-affine grain motion and the creation of contacts as the sample is compressed [37].

Dependence on the friction model.—To check if the memory effect could be an artifact of the friction model, simulations were carried out using three different models. A Hertzian repulsive normal force [46, 47] was used for all three models,

$$f_n = \max(0, k_n p^{3/2} + \gamma_n p^{1/2} \dot{p}) \quad (1)$$

as appropriate for viscoelastic rather than plastic grains [48–50]. Here p is the normal overlap of two grains, \dot{p} its rate of change, $k_n = 2^{-3/2}(4/3)R^{1/2}E/(1-\nu^2)$, and $\gamma_n/k_n = (0.23)t_c$ was used. Rolling at contacts is important in granular compressions [51, 52]; the rolling and twisting resistances were set to zero.

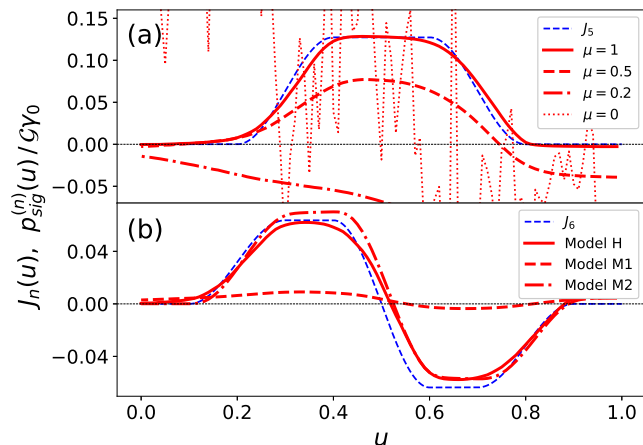


FIG. 5. Effects of varying the friction coefficient and the friction force model. In each case the response $p_{sig}^{(n)}(u)$ to a single input signal (I_5 or I_6) is shown, but the gain \mathcal{G} was adjusted as in Fig. 4 to minimize the errors summed over all six input signals. Details of this fitting procedure and the resulting \mathcal{G} values are in Supplementary Material [43]. (a) Effect of varying the grain-grain friction coefficient μ . The memory effect is essentially absent for $\mu \leq 0.2$, and when $\mu = 0$ numerous particle rearrangements make $p_{sig}^{(n)}(u)$ noisy. (b) Effect of varying the transverse force model. The simplest model H and the most realistic model for viscoelastic spheres M2 show similar memory effects, while the intermediate model M1 shows very little memory.

Friction models H, M1, M2 all include transverse elastic and damping force vectors \mathbf{f}_e , \mathbf{f}_d with the magnitude of the total transverse force limited by the Coulomb criterion $|\mathbf{f}_e + \mathbf{f}_d| < \mu f_n$ using the algorithm of Ref. [33].

Model H (“Hooke”) uses a linear spring and dashpot

$$\mathbf{f}_e = k_H \boldsymbol{\sigma}, \quad \mathbf{f}_d = \gamma_H \dot{\boldsymbol{\sigma}} \quad (2)$$

with $\boldsymbol{\sigma}$ is the accumulated vector sliding motion between the two grain surfaces and $\dot{\boldsymbol{\sigma}}$ its rate of change. Without the damping term this is the original friction model of Ref. [30]. Here k_H was set to a typical inverse transverse compliance [53] from model M1 below, and γ_H was set using $\gamma_H/k_H = (0.3)\gamma_n/k_n$. The data shown in Figs. 3-4 and 5(a) are for this simplest friction model H.

Model M1 (“Mindlin-1”) improves upon model H by making the transverse compliance dependent upon the normal overlap p , using a linearized, no-slip version [27] of the transverse force calculated by Mindlin and Deresiewicz for contacting elastic spheres [25, 54]. In this model the elastic force is accumulated using

$$\Delta \mathbf{f}_e = k_M p^{1/2} \Delta \boldsymbol{\sigma}, \quad \mathbf{f}_d = \gamma_M p^{1/2} \dot{\boldsymbol{\sigma}} \quad (3)$$

with $k_M = 3k_n(1-\nu)/(2-\nu)$ [37, 53]. As with model H $\gamma_M/k_M = (0.3)\gamma_n/k_n$ was used. To allow for the loss of stored elastic energy when p decreases, an approximation due to Walton is used [36, 50, 55]: the elastic force \mathbf{f}_e

is reduced proportionally to $p^{1/2}$. This model M1 has frequently been used for DEM simulations of frictional granular matter [36, 37, 55, 56].

Interestingly, when the nominally more realistic model M1 is substituted for model H, the memory effect reported here nearly disappears, Fig. 5(b). This can be traced to the approximation for the reduction of elastic energy, which effectively assumes that the current value of \mathbf{f}_e results entirely from sliding motion at the current value of p and thus erases memory of the degree of compression at which shear strains were applied to the sample.

Model M2 (“Mindlin 2”) avoids this approximation by directly computing the change of \mathbf{f}_e with decreasing overlap p from the linearized Mindlin model of Ref. [27]. One way to do this (used here) is to represent the transverse elastic force in a contact as an integral over contributions from sliding at different values of $q = p^{1/2}$, i.e. $\mathbf{f}_e = \int_0^\infty \mathbf{f}(q) dq$. The first of Eqs. 3 is implemented by adding $k_M \Delta \boldsymbol{\sigma}$ to $\mathbf{f}(q)$ in the interval $0 < q < p^{1/2}$, and when p decreases $\mathbf{f}(q)$ is set to zero for $q > p^{1/2}$. Note this is not a new friction model, but rather a more accurate representation than M1 of the transverse force law of Ref. [27]. Model M2 has not typically been used for DEM simulations because it requires keeping a (suitably discretized) vector-valued function $\mathbf{f}(q)$ of history information for each contact. This complex path history retention in each contact is an inherent property of the Mindlin-Deresiewicz theory [25, 27], but as the Model H results show it is not required for the bulk memory effect reported here.

With the more-faithful linearized Mindlin model M2, the memory effect is very similar to that seen for the simplest model H (Fig. 5(b)). Although friction models other than the three considered here have been used [32, 57, 58] models H and M2 are sufficiently different to suggest that the memory effect is insensitive to details of the model, provided it does not explicitly erase memories as M1 does.

The three models H, M1, M2 essentially assume grain-scale elasticity coupled with more microscopic Coulomb-law friction at contacting surfaces [53]. This should be valid for large elastomer grains, but harder, more sand-like granular media might not have this separation of scales. Recent work has explored microscopic, asperity-based models of friction for jammed granular media [59, 60], and it will be interesting to see if the memory effect reported here persists for such models. Also harder grain materials typically have smaller yield strains. Modeling them would require reducing the compression factor δ_0 , probably necessitating larger simulations to observe the shear strain memory as a bulk effect.

Conclusions.—It is found via simulations that random packs of soft, frictional grains effectively store for indefinite times input signals applied as small shear waveforms while the sample is slowly compressed, with the signals

recalled when the sample is eventually decompressed.

The proposed mechanism of memory formation is similar to holography, in that a local nonlinear phenomenon (contact friction) is used to record correlations between the input signal and a reference signal (the grain motions during compression). Re-application of the reference signal at a later time (by decompressing the sample) allows the memory to be read out.

The property of granular media that appears essential to such memory formation—the creation of internal, frictional contacts upon compression—exists for many other types of random media [2–8] which suggests that similar memory effects might be found more generally.

This work was completed in part with resources provided by the University of Massachusetts’ Green High Performance Computing Cluster (GHPCC).

* candela@physics.umass.edu

- [1] N. C. Keim, J. D. Paulsen, Z. Zeravcic, S. Sastry, and S. R. Nagel, Memory formation in matter, *Rev. Mod. Phys.* **91**, 035002 (2019).
- [2] Y. Bhosale, N. Weiner, A. Butler, S. H. Kim, M. Gazzola, and H. King, Micromechanical origin of plasticity and hysteresis in nestlike packings, *Phys. Rev. Lett.* **128**, 198003 (2022).
- [3] A. Panaitescu, G. M. Grason, and A. Kudrolli, Persistence of perfect packing in twisted bundles of elastic filaments, *Phys. Rev. Lett.* **120**, 248002 (2018).
- [4] A. Seguin and J. Crassous, Twist-controlled force amplification and spinning tension transition in yarn, *Phys. Rev. Lett.* **128**, 078002 (2022).
- [5] S. Poincloux, M. Adda-Bedia, and F. Lechenault, geometry and elasticity of a knitted fabric, *Phys. Rev. X* **8**, 021075 (2018).
- [6] K. Matan, R. B. Williams, T. A. Witten, and S. R. Nagel, Crumpling a thin sheet, *Phys. Rev. Lett.* **88**, 076101 (2002).
- [7] A. D. Cambou and N. Menon, Three-dimensional structure of a sheet crumpled into a ball, *PNAS* **108**, 14741 (2011).
- [8] Y. Lahini, O. Gottesman, A. Amir, and S. M. Rubinstein, Nonmonotonic aging and memory retention in disordered mechanical systems, *Phys. Rev. Lett.* **118**, 085501 (2017).
- [9] J. D. Paulsen, N. C. Keim, and S. R. Nagel, Multiple transient memories in experiments on sheared non-brownian suspensions, *Phys. Rev. Lett.* **113**, 068301 (2014).
- [10] D. Fiocco, G. Foffi, and S. Sastry, Encoding of memory in sheared amorphous solids, *Phys. Rev. Lett.* **112**, 025702 (2014).
- [11] S. Mukherji, N. Kandula, A. K. Sood, and R. Ganapathy, Strength of mechanical memories is maximal at the yield point of a soft glass, *Phys. Rev. Lett.* **122**, 158001 (2019).
- [12] N. C. Keim, J. Hass, B. Kroger, and D. Wieker, Global memory from local hysteresis in an amorphous solid, *Phys. Rev. Res.* **2**, 012004(R) (2020).
- [13] M. Toiya, J. Stambaugh, and W. Losert, Transient and oscillatory granular shear flow, *Phys. Rev. Lett.* **93**, 088001 (2004).
- [14] N. W. Mueggenburg, Behavior of granular materials under cyclic shear, *Phys. Rev. E* **71**, 031301 (2005).
- [15] J. Ren, J. A. Dijksman, and R. P. Behringer, Reynolds pressure and relaxation in a sheared granular system, *Phys. Rev. Lett.* **110**, 018302 (2013).
- [16] Y. Zhao, Y. Zhao, D. Wang, H. Zheng, B. Chakraborty, and J. E. S. Socolar, Ultrastable shear-jammed granular material, *Phys. Rev. X* **12**, 031021 (2022).
- [17] Y. Zhao, J. Barés, H. Zheng, J. E. S. Socolar, and R. P. Behringer, Shear-jammed, fragile, and steady states in homogeneously strained granular materials, *Phys. Rev. Lett.* **123**, 158001 (2019).
- [18] J. C. Burton and S. R. Nagel, Echoes from anharmonic normal modes in model glasses, *Phys. Rev. E* **93**, 032905 (2016).
- [19] J. A. Dijksman and T. Mullin, Creep control in soft particle packings, *Phys. Rev. Lett.* **128**, 238002 (2022).
- [20] C. S. O’Hern, L. E. Silbert, A. J. Liu, and S. R. Nagel, Jamming at zero temperature and zero applied stress: The epitome of disorder, *Phys. Rev. E* **68**, 011306 (2003).
- [21] E. Somfai, J.-N. Roux, J. H. Snoeijer, M. van Hecke, and W. van Saarloos, Elastic wave propagation in confined granular systems, *Phys. Rev. E* **72**, 021301 (2005).
- [22] A. J. Liu and S. R. Nagel, The jamming transition and the marginally jammed solid, *Annu. Rev. Condens. Matter Phys.* **1**, 347 (2010).
- [23] H. A. Makse, D. L. Johnson, and L. M. Schwartz, Packing of compressible granular materials, *Phys. Rev. Lett.* **84**, 4160 (2000).
- [24] I. Agnolin and J.-N. Roux, Internal states of model isotropic granular packings. II. Compression and pressure cycles, *Phys. Rev. E* **76**, 061303 (2007).
- [25] R. D. Mindlin and H. Deresiewicz, Elastic spheres in contact under varying oblique forces, *J. Appl. Mech.* **20**, 327 (1953).
- [26] D. Elata and J. G. Berryman, Contact force-displacement laws and the mechanical behavior of random packs of identical spheres, *Mech. Materials* **24**, 229 (1996).
- [27] D. L. Johnson and A. N. Norris, Rough elastic spheres in contact: Memory effects and the transverse force, *J. Mech. Phys. Solids* **45**, 1025 (1997).
- [28] J. A. C. Gallas and S. Sokolowski, Grain non-sphericity effects on the angle of repose of granular material, *Int. J. Mod. Phys. B* **7**, 2037 (1993).
- [29] T. D. Nguyen and S. J. Plimpton, Aspherical particle models for molecular dynamics simulation, *Comp. Phys. Comm.* **243**, 12 (2019).
- [30] P. A. Cundall and O. D. L. Strack, A discrete numerical model for granular assemblies, *Géotechnique* **29**, 47 (1979).
- [31] L. E. Silbert, D. Ertas, G. S. Grest, T. C. Halsey, D. Levine, and S. J. Plimpton, Granular flow down an inclined plane: Bagnold scaling and rheology, *Phys. Rev. E* **64**, 051302 (2001).
- [32] T. Pöschel and T. Schwager, *Computational granular dynamics, models and algorithms* (Springer, Berlin, 2005).
- [33] S. Luding, Cohesive, frictional powders: contact models for tension, *Granular Matter* **10**, 235 (2008).
- [34] H.-G. Matuttis and J. Chen, *Understanding the discrete element method* (Wiley, Singapore, 2014).
- [35] A. Haji-Akbari, M. Engel, A. S. Keys, X. Zheng, R. G. Petschek, P. Palffy-Muhoray, and S. C. Glotzer, Disordered, quasicrystalline and crystalline phases of densely

- packed tetrahedra, *Nature* **462**, 773 (2009).
- [36] I. Agnolin and J.-N. Roux, Internal states of model isotropic granular packings. I. Assembling process, geometry, and contact networks, *Phys. Rev. E* **76**, 061302 (2007).
- [37] H. A. Makse, N. Gland, D. L. Johnson, and L. M. Schwartz, Why effective medium theory fails in granular materials, *Phys. Rev. Lett.* **83**, 5070 (1999).
- [38] C. Thornton and S. Antony, Quasi-static shear deformation of a soft particle system, *Powder Tech.* **109**, 179 (2000).
- [39] A. Donev, R. Connelly, F. H. Stillinger, and S. Torquato, Unconstrained jammed packings of nonspherical hard particles: Ellipses and ellipsoids, *Phys. Rev. E* **75**, 051304 (2007).
- [40] S. Henkes, M. van Hecke, and W. van Saarloos, Critical jamming of frictional grains in the generalized isostaticity picture, *EPL* **90**, 14003 (2010).
- [41] It is not clear how relevant the concept of isotaticity is to the simulations reported here, as the grains are non-spherical, nonconvex, and compressible.
- [42] F. da Cruz, S. Emam, M. Prochnow, J.-N. Roux, and F. Chevoir, Rheophysics of dense granular materials: Discrete simulation of plane shear flows, *Phys. Rev. E* **72**, 021309 (2005).
- [43] Supplemental Material at XXX details the determination of the gain \mathcal{G} as well as a quantitative measure \mathcal{F} of the memory fidelity, and tabulates \mathcal{G} and \mathcal{F} values for each of the curves in Fig. 5.
- [44] K. A. Murphy, K. A. Dahmen, and H. M. Jaeger, Transforming mesoscale granular plasticity through particle shape, *Phys. Rev. X* **9**, 011014 (2019).
- [45] M. Kramár, L. Kovalcinova, K. Mischaikow, and L. Kondic, Quantitative measure of memory loss in complex spatiotemporal systems, *Chaos* **31**, 033126 (2021).
- [46] N. V. Brilliantov, F. Spahn, J.-M. Hertzsch, and T. Pöschel, Model for collisions in granular gases, *Phys. Rev. E* **53**, 5382 (1996).
- [47] T. Schwager and T. Pöschel, Coefficient of restitution for viscoelastic spheres: The effect of delayed recovery, *Phys. Rev. E* **78**, 051304 (2008).
- [48] O. R. Walton, Numerical simulation of inclined chute flows of monodisperse, inelastic, frictional spheres, *Mech. Materials* **16**, 239 (1993).
- [49] L. Vu-Quoc and X. Zhang, An elastoplastic contact force–displacement model in the normal direction: displacement-driven version, *Proc. R. Soc. Lond. A* **455**, 4013 (1999).
- [50] C. Thornton, S. J. Cummins, and P. W. Cleary, An investigation of the comparative behaviour of alternative contact models during inelastic collisions, *Powder Tech.* **233**, 30 (2013).
- [51] M. R. Kuhn and K. Bagi, Contact rolling and deformation in granular media, *Int. J. Solids and Structures* **41**, 5793 (2004).
- [52] Z. A. Benson, A. Peshkov, N. Yungler Halpern, D. C. Richardson, and W. Losert, Experimentally measuring rolling and sliding in three-dimensional dense granular packings, *Phys. Rev. Lett.* **129**, 048001 (2022).
- [53] K. L. Johnson, *Contact mechanics* (Cambridge Univ. Press, 1985).
- [54] R. D. Mindlin, Compliance of elastic bodies in contact, *J. Appl. Mech.* **16**, 259 (1949).
- [55] Tangential force model *mindlin_rescale/force* in the LAMMPS Molecular Dynamics Simulator, https://docs.lammps.org/pair_granular.html. Retrieved February 1, 2023.
- [56] H. A. Makse, N. Gland, D. L. Johnson, and L. M. Schwartz, Granular packings: Nonlinear elasticity, sound propagation, and collective relaxation dynamics, *Phys. Rev. E* **70**, 061302 (2004).
- [57] O. R. Walton and R. L. Braun, Viscosity, granular-temperature, and stress calculations for shearing assemblies of inelastic, frictional disks, *J. Rheol.* **30**, 949 (1986).
- [58] J. Schäfer, S. Dippel, and D. E. Wolf, Force schemes in simulations of granular materials, *J. Phys. I France* **6**, 5 (1996).
- [59] S. Papanikolaou, C. S. O’Hern, and M. D. Shattuck, Isostaticity at frictional jamming, *Phys. Rev. Lett.* **110**, 198002 (2013).
- [60] H. Ikeda, C. Brito, M. Wyart, and F. Zamponi, Jamming with tunable roughness, *Phys. Rev. Lett.* **124**, 208001 (2020).

Supplementary material for

“Complex memory formation in frictional granular media”

Determination of the gain and fidelity of the memory effect

It was found in the simulations that the shear stress $p_{sig}^{(n)}(u)$ measured while the sample was decompressed was approximately proportional to the integrated shear strain $\gamma_0 J_n(u)$ applied earlier while the sample was compressed,

$$p_{sig}^{(n)}(u) \approx \mathcal{G} (\gamma_0 J_n(u)) \quad (1)$$

for $n = 1 \dots N$, with $N = 6$ for the data shown in the main text. The proportionality factor or “gain” \mathcal{G} has units of pressure, and on dimensional grounds must itself be proportional to the grain modulus E . The gain \mathcal{G} was determined by minimizing squared error in Eq. 1 integrated over u and summed over input signals,

$$\mathcal{E}^2 = \sum_{n=1}^N \int_0^1 \left(p_{sig}^{(n)}(u) - \mathcal{G} \gamma_0 J_n(u) \right)^2 du. \quad (2)$$

Considering a set of N u -dependent functions to be a vector and defining the dot product

$$\{F_n(u)\}_{n=1\dots N} \leftrightarrow \mathbf{F}, \quad \mathbf{F} \cdot \mathbf{G} = \sum_{n=1}^N \int_0^1 F_n(u) G_n(u) du \quad (3)$$

the total error squared is

$$\mathcal{E}^2 = (\mathbf{p}_{sig} - \mathcal{G} \gamma_0 \mathbf{J}) \cdot (\mathbf{p}_{sig} - \mathcal{G} \gamma_0 \mathbf{J}). \quad (4)$$

Minimizing \mathcal{E}^2 by setting $d\mathcal{E}^2/d\mathcal{G} = 0$ finally yields

$$\mathcal{G} = \frac{1}{\gamma_0} \frac{\mathbf{J} \cdot \mathbf{p}_{sig}}{\mathbf{J} \cdot \mathbf{J}}. \quad (5)$$

We can also define a dimensionless “fidelity”

$$\mathcal{F} = 1 - \left(\frac{\mathcal{E}^2}{\mathbf{p}_{sig} \cdot \mathbf{p}_{sig}} \right)^{1/2} \quad (6)$$

which satisfies $0 \leq \mathcal{F} \leq 1$. If the recalled signals scaled by the optimized \mathcal{G} perfectly match the input signals then the fidelity is $\mathcal{F} = 1$, while conversely if the recalled signals are completely uncorrelated with the input signals $\mathcal{F} \ll 1$.

Dependence of the gain and fidelity on the friction coefficient and model

Friction coefficient. Apart from Fig. 5(b) all of the data shown in the main text were taken using the simplest (Cundall-Strack) friction model H. When the grain-grain friction coefficient μ was varied as shown in Fig. 5(a), the resulting gain and fidelity were as follows.

μ	\mathcal{G}	\mathcal{F}
1	1.77×10^5 Pa	0.910
0.5	1.85×10^5 Pa	0.676
0.2	2.18×10^5 Pa	0.229
0	-1.18×10^5 Pa	0.050

Each \mathcal{G} value was determined using all $N = 6$ input signals as described above, even though Fig. 5(a) only shows the results for input signal J_5 .

Examining this table it can be seen that the fidelity \mathcal{F} decreases monotonically with decreasing μ , becoming close to zero when grain-grain friction is turned off ($\mu = 0$). Conversely the best-fit gain \mathcal{G} does not have a clear trend with varying μ , but rather has a similar magnitude for all μ values. This indicates that as the friction coefficient is reduced, the magnitude of responses to the input signals remains roughly constant while the response waveforms become systematically less correlated with the input waveforms. In the limit $\mu \rightarrow 0$ the responses are effectively noise, which happens to be negatively correlated with the inputs for the particular random realization of the grain pack used in this case (indicated by $\mathcal{G} < 0$).

Friction model. For the data shown in Fig. 5(b) the friction model was varied, keeping all other parameters unchanged including $\mu = 1$. Hence the top line of this table is the same as the top line of the table above.

Model	\mathcal{G}	\mathcal{F}
H	1.77×10^5 Pa	0.910
M1	4.53×10^5 Pa	0.460
M2	5.46×10^5 Pa	0.891

As noted in the main text, the memory effect is strong ($\mathcal{F} \approx 0.9$) for models H and M2 while it is considerably weaker for model M1 with $\mathcal{F} = 0.46$. As shown in Fig. 5(b) this \mathcal{F} value corresponds to a markedly smaller response to the most complex input signal used, J_6 . A possible physical interpretation is that model M1 smears the response to the input at each u value across a range of u values in the recalled signal.

It can also be seen that the gain \mathcal{G} is about three times larger for model M2 than for model H. This is not surprising as the friction force laws (Eqs. 2 and 3 in the main text) are different, but the magnitude and direction of the difference in \mathcal{G} values are not explained.